CALOTRITON: A convective boundary layer height estimation algorithm from UHF wind profiler data

Alban Philibert, Marie Lothon, Julien Amestoy, Pierre-Yves Meslin, Solène Derrien, Yannick Bezombes, Bernard Campistron, Fabienne Lohou, Antoine Vial, Guylaine Canut-Rocafort, et al.

To cite this version:

Alban Philibert, Marie Lothon, Julien Amestoy, Pierre-Yves Meslin, Solène Derrien, et al.. CALOTRITON: A convective boundary layer height estimation algorithm from UHF wind profiler data. Journal of Environmental Radioactivity, 2023, 237, pp.106695. 10.5194/amt-2023-95 . hal-04625815

HAL Id: hal-04625815
https://hal.science/hal-04625815

Submitted on 28 Jun 2024

https://doi.org/10.5194/amt-2023-95
Preprint. Discussion started: 23 May 2023

Atmospheric Measurement Techniques
Discussions

CALOTRITON: A convective boundary layer height estimation algorithm from UHF wind profiler data

Alban Philibert[1,2], Marie Lothon[2], Julien Amestoy[3], Pierre-Yves Meslin[1], Solène Derrien[2], Yannick Bezombes[2], Bernard Campistron[2], Fabienne Lohou[2], Antoine Vial[2], Guylaine Canut-Rocafort[4], Joachim Reuder[5], and Jennifer Brooke[6]

[1]Institut de Recherche en Astrophysique et Planétologie, Université de Toulouse, CNRS, UPS, France
[2]Laboratoire d'Aérologie, Université de Toulouse, CNRS, UPS, France
[3]CEA, DAM, DIF, F-91297, Arpajon-Cédex, France
[4]CNRM-Université de Toulouse, Météo-France/CNRS, Toulouse, France
[5]Geophysical Institute, and Bergen Offshore Wind Centre, University of Bergen, and Bjerknes Center for Climate Research, Bergen, Norway
[6]Met Office, FitzRoy Way, Exeter, EX1 3PB, UK

Correspondence: Marie LOTHON (marie.lothon@aero.obs-mip.fr)

Abstract.

Long series of observation of the atmospheric dynamics and composition are collected at the French Pyrenean Platform for the Observation of the Atmosphere (P2OA). Planetary boundary layer depth is a key variable of the climate system, but it remains difficult to estimate and analyse statistically by use of long series. In order to obtain reliable estimates of the convective boundary layer height (Zi) and to allow long-term series analyses, a new restitution algorithm, named CALOTRITON, has been developed, based on the observations of a Ultra High Frequency (UHF) radar wind profiler (RWP) from P2OA, with the help of other instruments for evaluation. Zi estimates are based on the principle that the top of the convective boundary layer is associated with both a marked inversion and a decrease of turbulence. Those two criteria are respectively manifested by larger RWP reflectivity and smaller vertical velocity Doppler spectral width. With this in mind, we introduce a new UHF-deduced dimensionless parameter which weights the air refractive index coefficient with the inverse of vertical velocity standard deviation to the power x. We then search for the most appropriate local maxima of this parameter for Zi estimates, with defined criteria and constraints, like temporal continuity. Given that Zi should correspond to fair weather cloud base height, we use ceilometer data to optimize our choice of the power x, and find that $x = 3$ gives the best comparisons/results. The estimates of Zi by CALOTRITON are evaluated using different Zi estimates deduced from radiosounding, according to different definitions. The comparison shows excellent results with a regression coefficient of up to 0.96 and a root mean square error of 80 m, close to the vertical resolution of the UHF RWP of 75 m, when conditions are optimal. In more complex situations, that is when the atmospheric vertical structure is itself particularly ambiguous, secondary retrievals allow us to identify potential thermal internal boundary layers or residual layers, and help to qualify the Zi estimations. Frequent estimate errors are nevertheless observed when Zi is below the UHF RWP first reliable gate, but also at the end of the day, when the boundary layer begins its transition to a stable nighttime boundary layer.

1 Introduction

1.1 Zi definitions in CBL and associated instrumental techniques

The convective boundary layer (CBL) is defined as the lower layer of the troposphere where buoyancy mainly drives turbulence (Stull, 1988). CBL top (Zi) is a key variable in air quality since pollutants, dust, smoke,... emitted at the surface are mixed within this depth by dynamical and thermal turbulence. It is also a key variable for numerical weather predictions and climate models.

There are several definitions of Zi, depending on the points of view, notably: (i) thermodynamically, (ii) from the turbulence intensity, (iii) from the scalar concentration. Figure 1 schematizes those various definitions, through the vertical profiles of key variables.

The thermodynamic approach considers Zi as the height, from the surface, at which the somital inversion occurs, characterized by strong gradients of temperature and moisture (Fig. 1a, 1b). Several instrumental methods estimate Zi based on this approach, e. g. :

- the detection of gradients of either potential temperature, relative humidity or water vapor mixing ratio (e. g. Hennemuth and Lammert, 2006).
- the detection of the maximum of relative humidity (Couvreux et al., 2016).
- the so-called parcel method, which considers the potential temperature (or virtual potential temperature) at the surface θ_s, and searches for the height above surface where $\theta = \theta_s$ (Holzworth, 1964), or $\theta = \theta_s + \delta\theta$, where $\delta\theta$ is a small positive variation of surface potential temperature (Seibert et al., 2000) .

In-situ measurements from radiosounding, aircraft or remotely piloted aircraft systems (RPAS) can be used. Ultra High Frequency (UHF) radar wind profilers (RWPs), in L-band remote sensing, are also appropriate devices to detect the Zi sommital inversion associated with a significant increase of reflectivity (Angevine et al., 1994).

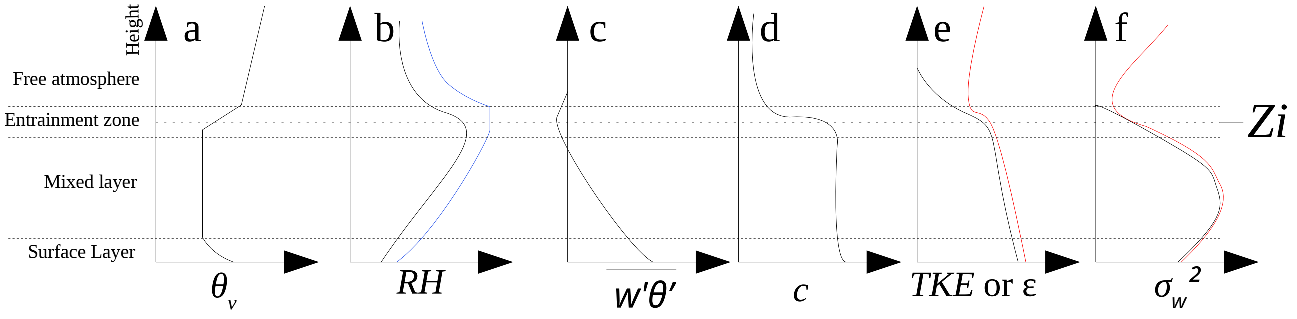

Figure 1. Idealized CBL profiles (black line) of (a) potential temperature, (b) relative humidity (blue line indicates the situation in the presence of clouds), (c) buoyancy flux, (d) scalar concentration, (e) turbulent kinetic energy (TKE) or turbulent dissipation rate (ε) and (f) vertical velocity variance (red line indicates the situation in the presence of external forcing).

The turbulence intensity approach considers Zi as the height, from the surface, where turbulence intensity starts to strongly decrease (Fig. 1e). This height is coupled with minimum (and negative) buoyancy flux (Deardorff, 1972) and decrease of vertical velocity variance (Stull, 1988). Both buoyancy flux and vertical velocity variance reach zero above Zi. But in case of external forcing like clouds, wind shear, advection, ..., a local minimum can be observed on each profiles (see red line Fig. 1e, 1f). Doppler lidar and UHF RWP give information on the turbulence intensity (Frehlich et al., 2006; Jacoby-Koaly et al., 2002, respectively). The variance of the Doppler velocity (Lothon et al., 2006), or the turbulent kinetic energy dissipation rate (e. g. Frehlich et al., 2006) can be used to detect the CBL top, based on a threshold.

The scalar concentration approach considers Zi as the height, from the surface, where strong discontinuity is observed in the scalar concentration profiles (Fig. 1d) like aerosol concentration. Optical remote sensing, like lidar and ceilometers, enable to access to aerosol concentration with the optical backscatter coefficient. Wavelet methods are typically used to detect the top of the more loaded CBL (e. g. Haeffelin et al., 2012), where the aerosol concentration abruptly falls from the CBL to the free troposphere (see e. g. Davis et al., 2000, for the use of the Haar-wavelet-based method). The mixing ratio maximum gradient method described above could also be considered as a scalar concentration approach.

Other approaches propose to use the combination of complementary instruments, like Min et al. (2020), with the use of the association of a microwave radiometer with ceilometer. Some studies compare the various methods and instrumental approaches, e. g. Couvreux et al. (2016), or Duncan et al. (2022). The latter discuss the wether conditions for which the various instruments are the most appropriate. In their study, RWP is found to give robust results, with a small bias relative to the radiosoundings, and a decrease of performance in the presence of clouds (due to the presence of turbulence in clouds).

Since they are based on different definitions, all the methods mentioned before potentially result in slightly different estimates of Zi (Caicedo et al., 2017), especially when the observed CBL is not as simple as in a textbook.

Here, we revisit the methodology of estimating Zi from UHF RWP measurements.

1.2 Main objectives

As one of the multi-instrumented site of the ACTRIS-Fr[1] infrastructure, the Pyrenean Platform for the Observation of the Atmosphere (P2OA2[2] – Lothon et al., 2023) gathers a comprehensive set of instruments for the monitoring of the atmosphere, all located at the Center for Atmospheric Research (CRA), Campistrous, France. Among them, a UHF RWP has continuously documented the Planetary Boundary Layer since 2010. Retrieving the CBL height from this instrument over this ongoing long series would allow statistical study of the dynamical processes in this mountainous region, such like: the influence of plain-mountain circulations, in link with thermally-driven winds; the interaction between mountain waves and boundary layer; impact of mesoscale subsidence related to orographic convection. It would also enable us to make statistical analysis and climatologies, with applications in air quality, weather forecasting and climate studies.

An existing technique based on Angevine et al. (1994) was used so far for the estimate of Zi with this instrument. It is known that this technique gives very satisfying results on a case-by-case investigation for fair weather convective conditions without

---

[1] ACTRIS-Fr is the French component of the European Aerosol, Cloud and Trace Gases Research Infrastructure (ACTRIS), https://www.actris.fr/

[2] https://p2oa.aeris-data.fr/

https://doi.org/10.5194/amt-2023-95
Preprint. Discussion started: 23 May 2023

complex vertical structure of the atmosphere (Heo et al., 2000). However, this technique is not robust enough for statistical studies based on long series. One obvious limitation for example, is that it often catches the top of the residual layer in early morning, rather than the top of the new thiner developing CBL top. Here, we propose to improve the method, and develop a new algorithm that would be able to deal with much more general conditions, including complex vertical structure of the atmosphere, cloudy situations and multi-layered low troposphere.

We present the experimental data used in Sect. 2, describe the Zi-retrieval algorithm (CALOTRITON) and discuss the choice of configuration parameters in Sect. 3, analyse the results and compare the CALOTRITON UHF-based Zi-estimates to in-situ measurements in Sect. 4. Conclusions and perspectives are drawn in Sect. 5.

2 Instrumentation and data

2.1 Datasets

In this study, we consider the data of the P2OA UHF RWP to develop the new CALOTRITON algorithm, for the retrieval of the CBL heigh throughout the whole 22 year long and ongoing time series of observations. We also use the data from the P2OA 60 m tower instrumented to provide vertical profiles of turbulence and meteorological data in the surface layer. Table 1 summarises all the instruments used in this study, their location, context, measurement period and dataset reference.

Table 1. Summary of instruments used and datasets

Instrument	Location	Context	Period	Reference
P2OA UHF RWP	P2OA-CRA	P2OA observatory	2015-2022	Lothon et al. (to be specified)
		BLLAST	June to July 2011	Saïd (2012)
	Els Plan, Spain	LIAISE	July 2021	Lothon and Vial (2022)
CNRM UHF RWP	Capvern, France	BLLAST	June to July 2011	Garrouste (2011)
	La Cendrosa, Spain	LIAISE	July 2021	Vial (2023)
Radiosoundings	P2OA-CRA	BLLAST	June to July 2011	Lothon (2018)
	Capvern, France			Legain (2011)
	Els Plan, Spain	LIAISE	July 2021	Price (2023b)
	La Cendrosa, Spain			Garrouste et al. (2022)
Remotely Piloted Airplane System	P2OA-CRA	BLLAST	June to July 2011	Reuder and Jonassen (2017)
	Capvern, France			
Instrumented towers	P2OA-CRA	P2OA observatory	2015-2022	Lohou et al. (to be specifieda, t)
		BLLAST	June to July 2011	Lohou (2017)
	Els Plan, Spain	LIASE	July 2021	Price (2023a)
	La Cendrosa, Spain			Canut et al. (2022)
CT25k Ceilometer	P2OA-CRA	P2OA observatory	2016-2019	see *Data availability*

To optimize CALOTRITON parameters, we compare Zi estimates with cloud base heights (Sect. 3.3) measured by the CT25k ceilometer from Centre National de Recherche Météorologique (CNRM), installed from December 2016 to December 2019 at P2OA-CRA.

The algorithm results are validated (see Sect. 4.2) by comparison to in-situ radiosonde and Remotely Piloted Airplane System (RPAS) measurements during two intensive measurement campaigns BLLAST (Boundary Layer Late Afternoon and Sunset

Turbulence, Lothon et al., 2014), which took place at P2OA-CRA and LIAISE (Land surface Interactions with the Atmosphere over the Iberian Semi-arid Environment, Boone et al., 2021), which took place in Spain, close to Lleida. The latter enables us to test CALOTRITON in another meteorological and geographical context than for the long term observational record of P2OA, and thus generalize its applicability and use. For both measurement campaigns, the CNRM UHF RWP is used in addition to the P2OA UHF RWP which also allows to test the algorithm on different UHF RWP.

2.2 UHF RWP measurement example

In this section, we present two study cases to illustrate our motivations to improve the current methods of Zi retrieval from a UHF RWP: one simple clear sky case (27 October 2021) and one more complex (15 March 2018).

The P2OA UHF RWP is a wind profiler with 5 beams, four oblique beams and one vertical beam. Its main characteristics are detailed in Table 2 (for more details, see Jacoby-Koaly, 2000).

Table 2. Main characteristics of the P2OA UHF RWP (https://p2oa.aeris-data.fr/sedoo_instruments/profileur-de-vent-uhf/). The CNRM UHF RWP present the same characteristics but with a first level with a good confidence index of 300 m.

Manufacturer	Degreane
Reference	PCL1300
Number of beams	5 (NWSE+vertical)
Transmission Frequency	1274 MHz
Opening Angle	8.5°
Obliques antennas inclinaison	17° to the vertical
Vertical Resolution	75 m
Temporal Resolution	$\sim$ 2 minutes
First level with a good confidence index	225 m

Figure 2 (panels a to e) shows different parameters measured by the UHF RWP in a clear sky case on 27 October 2021 at P2OA-CRA. The 3 components of the wind are deduced from the Doppler radial velocity of the 5 beams, every 75 m, and every 2 minutes. The air refractive index structure coefficient C_n^2 (Fig. 2c) is deduced from the reflectivity as a function of the received power (Doviak and Zrnic, 1993). The vertical velocity variance σ_w^2 (Fig. 2d) is obtained from the spectral half width of the backscattered signal and allows an estimate of the turbulent kinetic energy (TKE) dissipation rate ε (Fig. 2e) (Cohn and Angevine, 2000; Jacoby-Koaly et al., 2002). Here, C_n^2 is the median air refractive index structure coefficient over the 5 beams, as a function of altitude and time. ε is the median TKE dissipation rate over the 5 beams. σ_w is deduced from vertical antenna and corrected for the effect of the horizontal wind within the antenna aperture.

Figure 3 (panels a to g) compares in-situ measurements of thermodynamical variables measured by radiosondes with the UHF RWP variables at 13:35 UTC, on the same day of UHF RWP observations shown in Fig. 2.

Angevine et al. (1994) propose a CBL top retrieval method based on UHF RWP measurements, by assigning Zi at the height of the maximum reflectivity for each profile. Figure 3d indeed shows that the maximum reflectivity corresponds well to the CBL top, characterized by a strong gradient of potential temperature and mixing ratio (Fig. 3a and 3b). It indeed shows that σ_w^2 (Fig. 3e) and ε (Fig. 3f) are small at this height, leading to a local minimum. In "ideal" clear days, without external forcing, we

https://doi.org/10.5194/amt-2023-95
Preprint. Discussion started: 23 May 2023

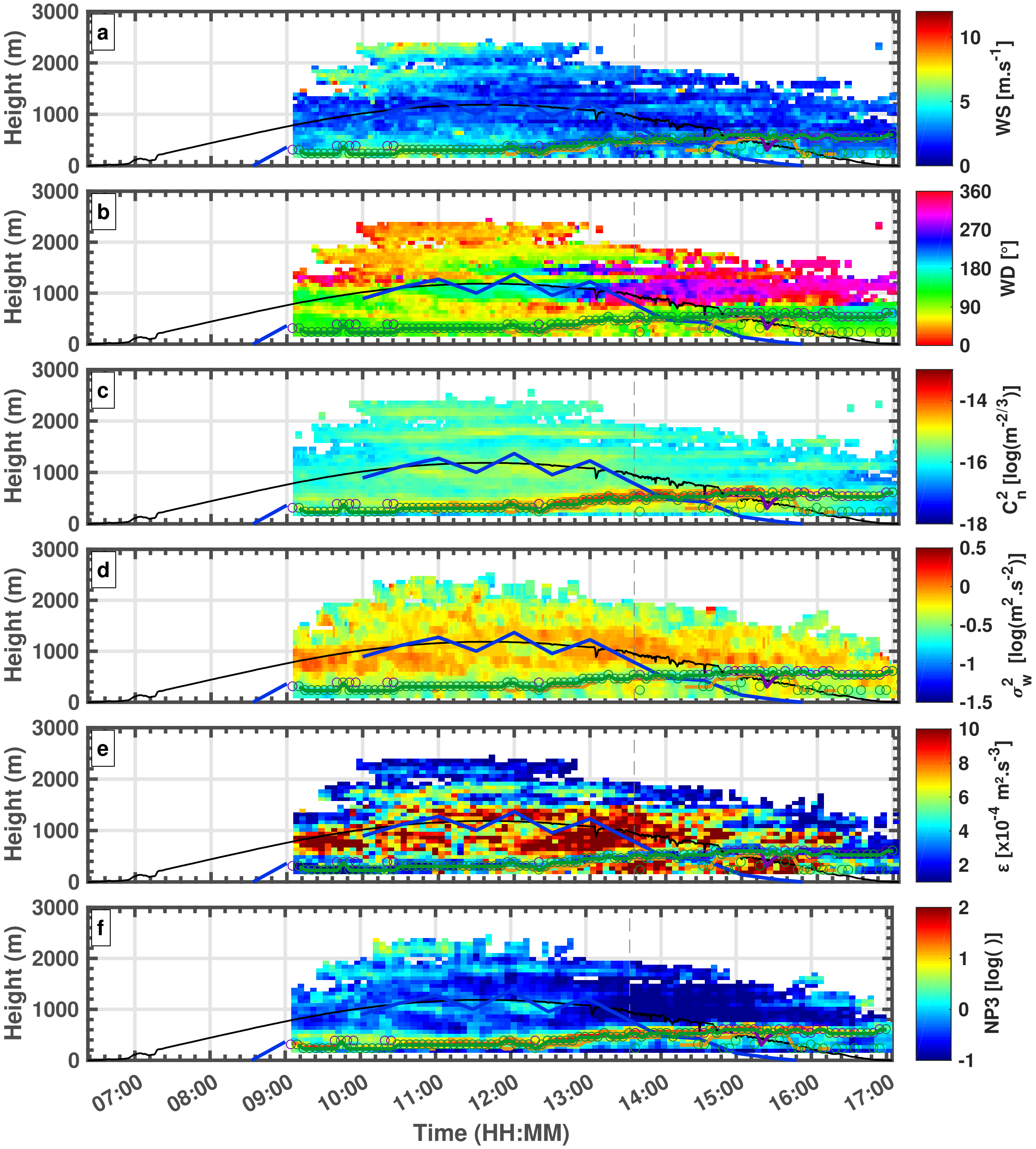

Figure 2. UHF RWP observations for 27 October 2021 at P2OA-CRA during clear sky: (a) wind speed (WS), (b) wind direction (WD), (c) filtered C_n^2 in log scale, (d) filtered σ_w^2 in log scale, (e) filtered and integrated ε in log scale, (f) integrated $NP3$ in log scale. For all panels, Zi estimates as described in Sect. 3.2.2 and 3.3.3: Zi_ε (orange line), $Zi_{NP0_{std}}$ (purple line), $Zi_{NP0_{sup}}$ (purple circles), $Zi_{NP3_{std}}$ (green line), $Zi_{NP3_{sub}}$ (green circles); and based on the same ordinate axis (but with different units): short wave down (W m^{-2}) (black line), sensible heat flux (deciW m^{-2}) (blue line). The vertical dashed line correspond to the time of the discussed radiosounding.

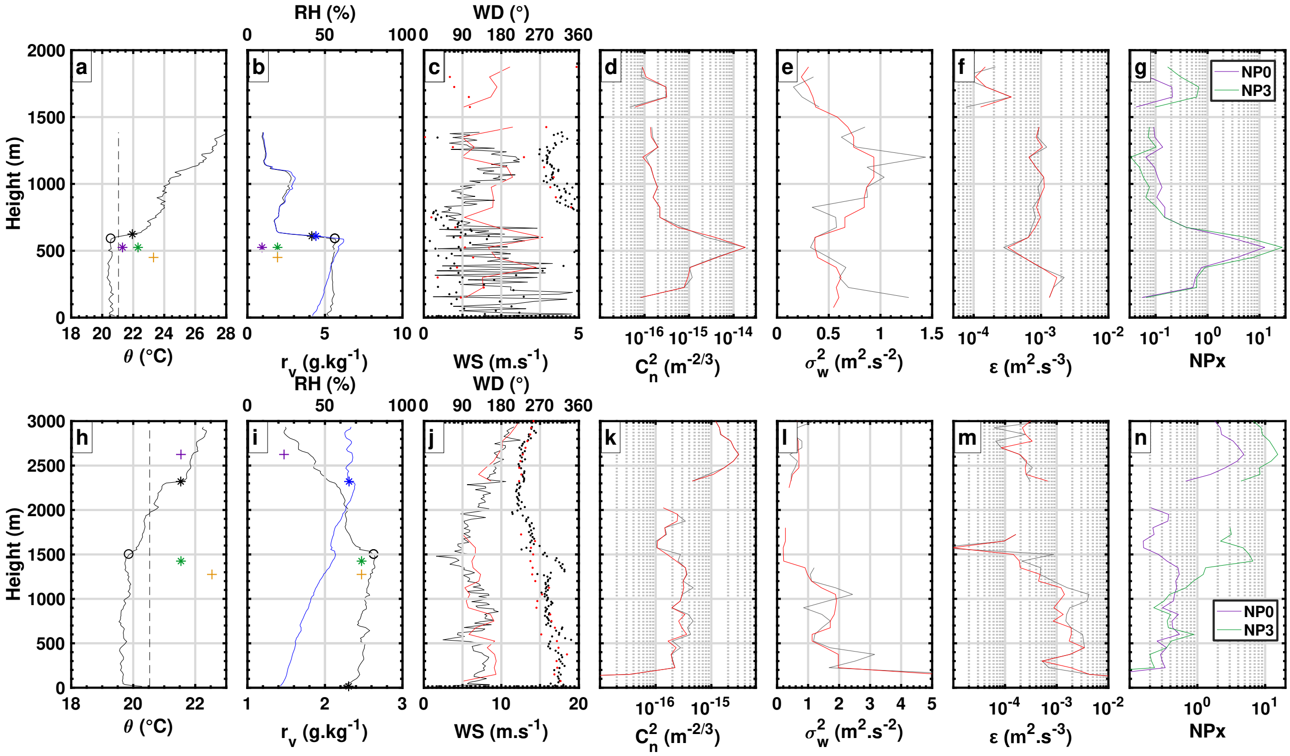

Figure 3. Profiles measured by radiosondes and UHF RWP at P2OA-CRA, on 27 October 2021, at 13:35 UTC: (a)potential temperature (black solid line), surface potential temperature + 0.25°C (black dashed line), Zi from in-situ subjective method (black circle), Zi from in-situ potential temperature gradient method (black asterisk), $Zi_{NP0_{std}}$ (purple '×'), $Zi_{NP0_{sup}}$ (purple '+'), $Zi_{NP3_{std}}$ (green '×'), $Zi_{NP3_{sub}}$ (green '+'), Zi_{ε} (orange '+'); (b) mixing ratio (black line) and relative humidity (blue line), Zi from in-situ mixing ratio gradient method (black asterisk), Zi from in-situ relative humidity gradient method (blue asterisk), purple, green and orange crosses same as described in (a); (c) wind speed (solid line) and wind direction (dottet line) from radiosonde (black) and UHF RWP (red); (d) air refractive index structure coefficient from UHF RWP with raw data (grey line) and filtered data as described in Sect. 3.2.2 (red line); (e) vertical velocity variance from UHF RWP with same colour code as (d); (f) TKE dissipation rate from UHF RWP with same colour code as (d); (g) NP0 (purple line) and NP3 (green line); (h) to (n) same as (a) to (g) respectively on 15 March 2018, at 14:15 UTC.

would typically not observe significant turbulence above Zi (Fig. 1e). In this case, forcing is small, with weak wind (Fig. 2a) but the wind shears (Fig. 2b) still generates significant turbulence (Fig. 2e).

Figure 4 (panels a to e) gives another example of UHF RWP measurements on 15 March 2018, this time with a marked external forcing, identified by a cloudy sky and by a high wind speed in the upper layer.

Figure 3 (panels h to n) confronts in situ measurements of thermodynamical variables with the UHF RWP variables at 14:15 UTC that same day. In this case, the reflectivity maximum (at $\sim$ 2500 m a. g. l.) does not correspond to Zi (see Fig. 3k) which is assumed to be around 1500 m a. g. l. where the potential temperature gradient (Fig. 3h) becomes positive (stable layer) while the maximum of C_n^2 actually corresponds to the cloud base (see the black points in Fig. 4). However, the local minima of σ_w^2 and ε are well associated with Zi (Fig. 3l and 3m).

https://doi.org/10.5194/amt-2023-95
Preprint. Discussion started: 23 May 2023

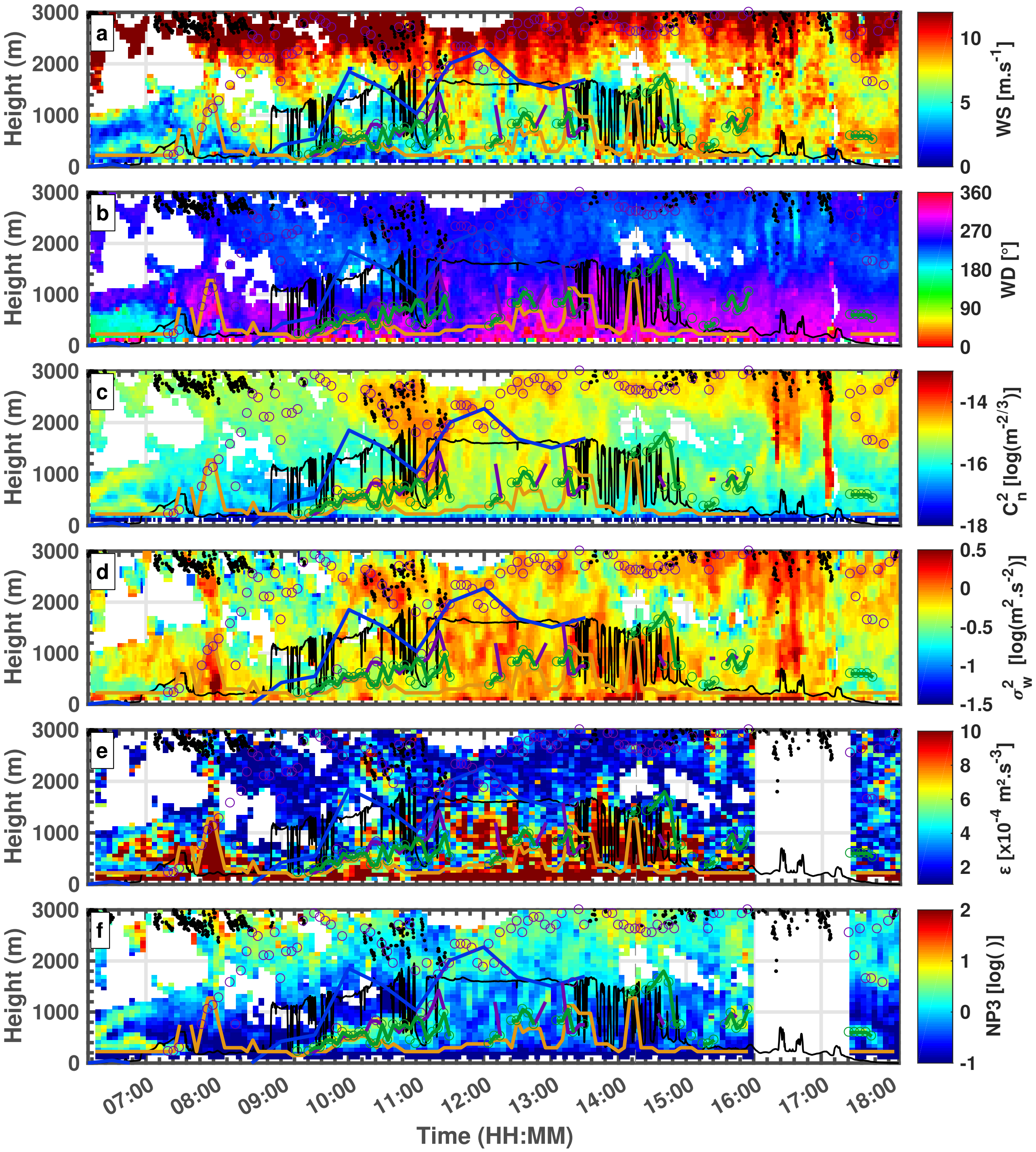

Figure 4. P2OA UHF RWP observations for 15 March 2018 at P2OA-CRA with the same description as Fig. 2 and cloud base height measured by CT25k ceilometer (black points).

https://doi.org/10.5194/amt-2023-95
Preprint. Discussion started: 23 May 2023

Moreover, we can see between 15:00 UTC and 17:00 UTC in Fig. 4c the presence of virga (verified by observations of the weather radars of Meteo-France). With droplet size close to the RWP wavelength, this induces a strong reflectivity (and C_n^2) on the entire profiles.

3 The CALOTRITON algorithm

3.1 Specific CALOTRITON objectives

In order to obtain reliable Zi estimates with UHF RWP and to allow long time series analysis of the P2OA-CRA dataset, a Zi-retrieval algorithm (CALOTRITON) was developed with 5 main objectives and constraints:

1. To restrict Zi estimate to the convective boundary layer, by only considering daytime conditions and excluding precipitation periods.
2. To respect temporal continuity of Zi growth and to follow it as finely as possible in time, in order to describe the smallest convective scales (5 to 30 minutes, Stull, 1988). Zi should start close to the ground early in the day.
3. To manage complex cases: as in the presence of clouds (as shown as Fig. 4), or thermal internal boundary layer (TIBL), when cold air advection in the lower layers can create a new convective boundary layer e. g., in case of slope wind (Kossmann et al., 1998) or sea breeze (Durand et al., 1989).
4. To take into account abrupt CBL growth, which occurs in the presence of a residual neutral layer above Zi, when the current CBL potential temperature gets to reach the residual neutral layer potential temperature (Blay-Carreras et al., 2014).
5. To use limited instrumental synergy in order to apply it in other sites (or measurement campaigns) equipped with a UHF RWP, and not to depend on the availability of an advanced instrument suite to establish Zi estimate.

3.2 CALOTRITON operation

Figure 5 presents a scheme of CALOTRITON algorithm which is described in details below.

3.2.1 Restriction to CBL conditions

First, we consider UHF RWP data only above 225 m a. g. l.. This is the first gate where data are always of high quality. Only daytime data are selected to estimate Zi from the UHF RWP. For this, sunrise and sunset times are retrieved as a function of date, altitude, latitude and longitude.

Precipitation periods (including virga) are excluded by a function based on empirical thresholds on C_n^2 and Doppler vertical velocity (w). Any profile which meets $C_n^2 > 10^{-14}$ m$^{-2/3}$ and $w <$ - 1 m s^{-1} over five consecutive levels is removed, as well as all profiles occurring 15 minutes before and after (see Fig. 4c bewteen 16:00 UTC and 17:00 UTC). We do not assign Zi

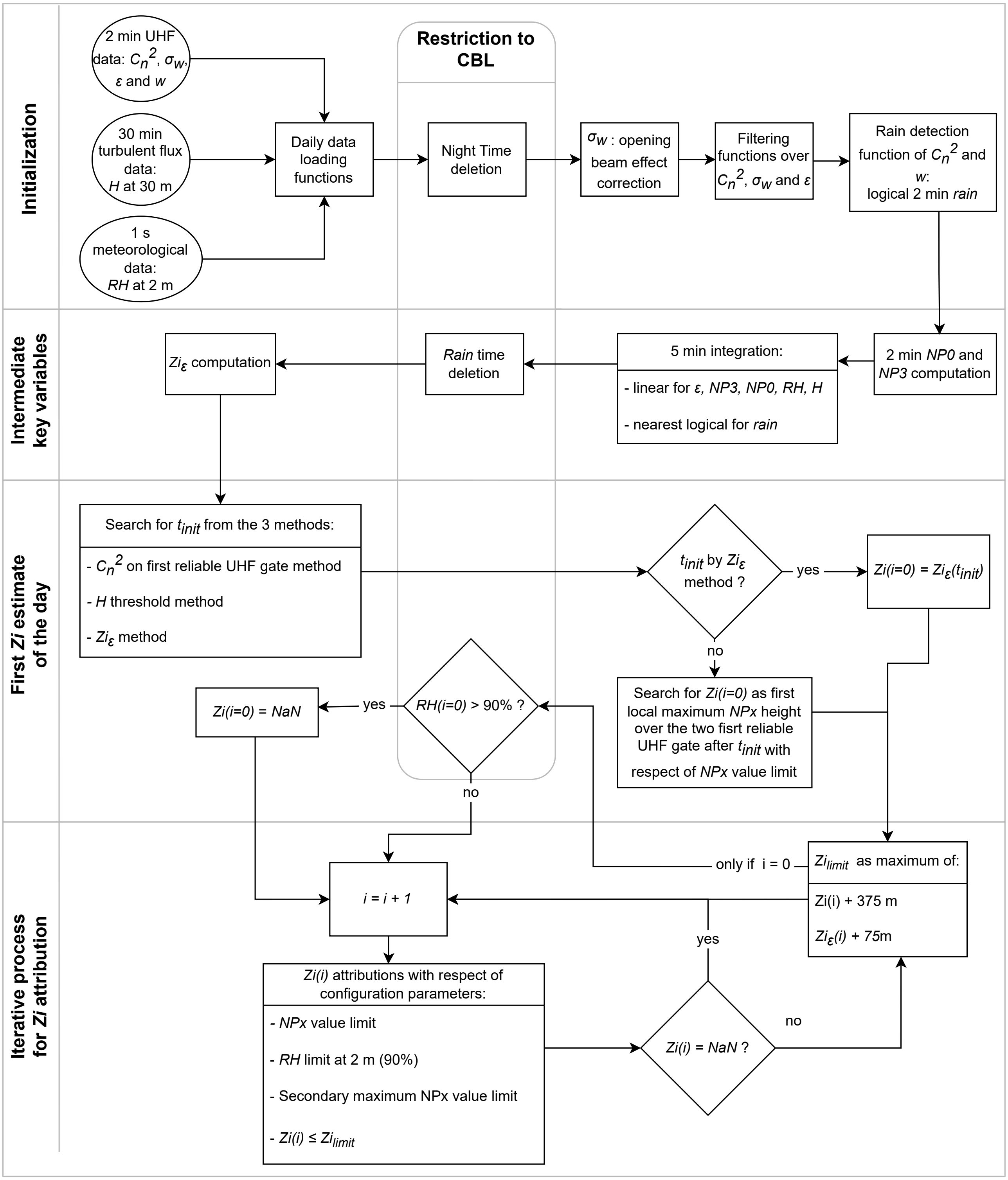

Figure 5. CALOTRITON organisation chart.

https://doi.org/10.5194/amt-2023-95
Preprint. Discussion started: 23 May 2023

in case of fogs, notably due to the limitation of the UHF RWP below 225 m a. g. l.. It was found at P2OA site that relative humidity at 2 m larger than 90 % was associated to fog occurence as confirmed by ceilometer measurements (not shown). We therefore take this as criterium for fog occurrence, and remove corresponding periods from the further analysis.

3.2.2 Definition of intermediate key variables

As the reflectivity maximum does not always correspond to Zi, especially in the case of a cloudy sky, we suggest using a new dimensionless variable which takes into account both, the increase of reflectivity at the sommital inversion and the decrease of turbulence: NPx (eq. 1) weights C_n^2 by σ_w power x, and allows for a better account of a large value of C_n^2 associated with a small value of σ_w. Dimensionless NPx is obtained by averaging values of C_n^2 and σ_w^x in the vertical for each profile (overlines in eq. 1):

$$NPx = \frac{C_n^2/\overline{(C_n^2)}}{\sigma_w^x/\overline{\sigma_w^x}} \tag{1}$$

The choice of x is discussed in the Sect. 3.3.2. As examples, Figures 2f and 4f show cross sections of $NP3$ for the examples discussed previously.

In order to disregard non-meterorological disturbances (e. g., birds) on the UHF RWP signal, C_n^2, σ_w and ε data are filtered by complementary sliding median filters:

- C_n^2 and ε: median over 6 minutes (3 points), none over height in order to keep the original UHF RWP vertical resolution of 75 m (dz).

- σ_w : median over 8 minutes (4 points), and a median over 225 m (3 points), because of a more pronounced spatio-temporal variability of these data (see Fig. 2d, 4d 7d). We use coarser filters for σ_w to compensate for the fact that C_n^2 and ε are already integrated over the 5 beams.

NPx is computed with these filtered data and linearly integrated over a 5 minute time step to describe the smallest characteristic convective scale. If a larger integrated time is chosen, the corresponding median time filter should be adujsted and applied to C_n^2, ε and σ_w.

We also consider another variable, purely defined by the level of turbulence: Zi_ε is the height above the surface at which the TKE dissipation rate ε falls below 5×10^{-4} m^2 s^{-3}. It thus represents a rough estimate of the depth of significant turbulence. Zi_ε is computed on filtered and integrated ε data (5 minutes as NPx). In order to consider only the Zi_ε that would respect a certain temporal continuity, a sliding median filter over 15 minutes (3 points) is applied on Zi_ε.

NPx is the core variable of CALOTRITON, but Zi_ε will help us on documenting the associated turbulence, and optimize the selection of the most appropriate local maximum of NPx as an estimate of Zi (we hereafter call this selection "Zi attribution"

3.2.3 Determination of the first Z_i estimate of the day

In a typical CBL development, Zi starts close to the ground, below the UHF RWP detection limits (225 m), and grows until it reaches a plateau in the early afternoon (Stull, 1988). It is therefore necessary to wait for some time (called t_{init}) before Zi can be detected by the UHF RWP. We found that the sensible heat flux, which governs the evolution of Zi, remains very low (less than a few tens of W) at least until an hour and a half after sunrise (not shown). Therefore, t_{init} is not defined before 1.5 hour after sunrise.

Several methods are used to determine t_{init}. The first is based on C_n^2 at the first reliable UHF RWP gate (225 m a. g. l.) and considers t_{init} as the time when the 30-minute sliding median exceeds its daily mean value. That way, it is investigated when an increase in C_n^2 becomes significant and may correspond to Zi. The second method is based on the measured sensible heat flux (H) and considers t_{init} when H exceeds a significant threshold of 50 Wm^{-2}. t_{init} is taken as the earliest time over those two. The first assigned Zi of the day can only be established at a local maximum of the vertical profile of NPx located at one of the two first reliable levels of the UHF RWP and occurring after t_{init}.

Sometimes, a thin layer is mixed by dynamical turbulence before sunrise, e.g., in the presence of a low level jet. In order to take those situations into account, we allow the attribution of the first Zi at the height of Zi_ε if the latter corresponds exactly to the height of the NPx maximum of the profile, independently of t_{init}, and provided that this attribution is always done 1.5 hour after sunrise.

3.2.4 Iterative process for Zi attribution

Once the initial Zi is found, the search for subsequent Zi is done by temporal iteration on the most significant local maximum of NPx that is located within a vertical growth limit of 375 m since its last effective attribution. Residual layers or clouds above Zi can potentially return a higher signal contribution to NPx than Zi itself, and might be misinterpreted if located within the 375 m growth limit. To take this into account, the algorithm allows attributions on local secondary maxima of NPx below the first if the value of the corresponding NPx is at least 90 $\%$ of the first maximum value of NPx before 10:00 UTC and 50 $\%$ after. These empirical values are discussed in section 3.3.2 and named relative thresholds of secondary maximum of NPx. Finally, a minimal value of NPx is required for attribution and fixed to the mean profile value of NPx in order to take into account a certain significance.

Sometimes, strong growth of Zi can occur and exceed the imposed limit (375 m). This motivated us to use Zi_ε, in order to consider up to which level significant turbulence is found. If at i time, $Zi_\varepsilon(i)$ is higher than the last effective attribution plus the growth limit, then $Zi(i)$ can be searched up to Zi_ε(i) + dz (where dz = 75 m).

3.3 Algorithm parameter choice

3.3.1 Parameter optimization

All the parameters presented above were obtained empirically by subjectively judging the quality of the attributions of Zi for about 100 days in 2018 at P2OA-CRA. In order to verify their quality in a more objective way and possibly to adjust some parameters, we compared the estimates of Zi with the lowest cloud base height measured by the CT25k ceilometer within a 5-minute interval around each attribution. This comparison is based on data from December 2016 to December 2019. When comparing two configurations with the distributions shown in Fig. 6, one would favour the configuration which leads to less attributions above cloud base and lower values of ε at Zi.

Figure 6 shows an example of the results of this comparison, for Zi estimates based on either $NP3$ or $NP0$, with the use of the optimal parameters listed in Table 3. Figure 6a shows the distribution of the set of Zi attributions for the different NPx (x=0 and x=3), and indicates more attributions by $NP3$, especially for Zi < 700 m. Figure 6b shows the distribution of the differences between Zi and CBH.

It can be seen that there are slightly more attributions above the cloud base when using $NP0$. Figure 6c presents the distribution of all ε values at Zi height, and shows that $NP3$ attributions tend to get lower ε values at Zi height. The fact that $NP3$ attributions of Zi are more often lower than $NP0$ attributions and associated with lower ε values is a sign of better quality attributions.

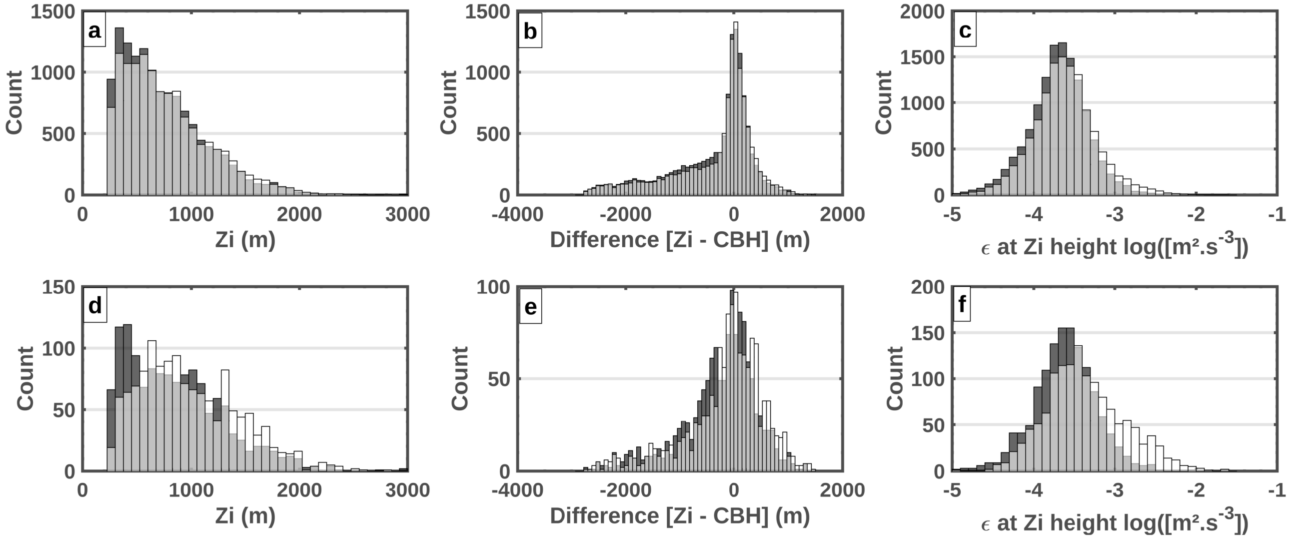

Figure 6. Histograms showing the differences between the distributions of $Zi_{NP0_{std}}$ (white bar) and $Zi_{NP3_{std}}$ (black bar) in presence of cloud measured by the CT25k ceilometer from december 2016 to december 2019: (a) Zi distribution, (b) distribution of difference between Zi and cloud base height; (c) ε value distribution at Zi height. (d) to (f) are respectively the same as (a) to (c) but considering only attributions which present more than 225 m difference between $Zi_{NP0_{std}}$ and $Zi_{NP3_{std}}$.

When clouds are present, the difference amount between Zi estimates with $NP3$ and $NP0$ is on average twice as large as in clear sky cases, due to the complexity of the atmosphere in cloudy conditions. Thus, the observed differences between Zi attributions with $NP3$ and $NP0$ give an indication of the CBL complexity.

Figure 6d to 6f presents the same figure as the top panel (Fig. 6a to 6c) but only considering the attributions by $NP3$ and $NP0$ when they differ for more than 225 m from each other. This represents only 10 % of the total attributions. The same conclusions as previously stated can be drawn, even more clearly here. We therefore confirm that $NP3$ statistically gives better results.

3.3.2 Tested parameters and optimum set

In this way, the set of NPx for x = 1 to 5 were compared two by two with the configuration presented in Table 3. It was noted that attributions were potentially better for x = 3 rather than x = 0, 1 or 2. However, no significant trend was noticed for $x \geq 3$. We limit us to x = 3 in order to keep attributions more based on C_n^2 than σ_w.

In this section, only a few results of our search for the best parameters by attribution distribution analysis are presented. All are based on $NP3$. The largest differences appeared between whether or not we consider the limit on relative humidity. Not setting a limit allows about 4% more attributions in clear sky and 40% more in the presence of clouds. Among those 40%, half of them corresponds to cloud base heights below 225 m, which is the first level of the UHF RWP. Considering the limit on relative humidity, 13% of all attributions in the presence of clouds take place 225 m above the cloud base, compared to 22% without a limit. This limit therefore both avoids attributions in the presence of clouds whose base is below the UHF RWP lower limit and reduces the number of attributions above the cloud base by half.

The methods for the search of t_{init} were tested. Using solely the C_n^2 maximum technique leads to almost no difference in Zi attributions, but using aditionnally the technique based on sensible heat flux leads to 3% more attributions.

Other values related to the growth limit were also tested. It was noticed that a limit of 300 m with the last effective attribution potentially allows to obtain better quality attributions but leads to a reduction of 3% of the attributions compared to a limit

Table 3. List of best parameters for CALOTRITON configuration

Parameter	Value	Comments
Integration time	5 minutes	
Time median filter C_n^2	3 points	$\sim$ 6 minutes
Time median filter ε	3 points	$\sim$ 6 minutes
Time median filter σ_w	4 points	$\sim$ 8 minutes
Height median filter C_n^2	0 points	0 m
Height median filter ε	0 points	0 m
Height median filter σ_w	3 points	225 m
Growth limit	375 m	between two effective assignments
Relative humidity limit at 2m	90 %	
NPx Value limits	NPx profile mean	
Secondary maximum NPx value limit	90% before and 50% after 10:00 UTC	And respect NPx Value limit
Zi_ε option	True	To exceed the growth limit

of 375 m. Empirically, it was found that 300 m was not sufficient to properly track the evolution of Zi compared to 375 m. On the other hand, a 450 m growth threshold dit not improve statistically the results. Although it leads to an increase of the total number of attributions by 3%, all additional attributions under cloudy skies were above cloud base. This is the reason we finally chose 375 m as the optimal growth threshold.

Other important parameters are the values selected for the relative thresholds of secondary maximum NPx on which attributions are possible. Not setting a limit leads to an increase of 40% in attributions above CBH + 225 m, associated with higher ε values, which is thus less appropriate. Thresholds of 50% and 90% were tested over the whole day and it was found that 50% led to more attributions over residual layers than 90%, especially in the morning. In contrary, a threshold of 90% leads to more attributions inside the CBL, especially in the afternoon. This is why a threshold of 90% before 10:00 UTC and 50% afterwards was chosen. A threshold of 75% for the whole day was also tested but provided poorer results.

3.3.3 Final assignment and flags

As we have seen previously, the difference between $NP0$ and $NP3$ attributions with the parameter set as described in Table 3, gives a useful and complementary information about the complexity of the lower troposphere. This is why we perform four estimates of Zi:

- $Zi_{NP3_{std}}$: estimated with standard configuration for $NP3$ as described in Table 3, considered as the best attributions.
- $Zi_{NP0_{std}}$: estimated with standard configuration for $NP0$ as described in Table 3
- $Zi_{NP0_{sup}}$: estimated for $NP0$ as described in Table 3, but without the relative humidity limit at 2m and NPx value limit, no possibility to take into account a secondary maximum of NPx, no t_{init} restriction (only after sunrise), and 375 m growth limit between the searched Zi and the maximum Zi already allocated with this configuration. This configuration allows to search for levels higher than the estimates made with a standard configuration, which could correspond to Zi if the standard configurations assign on a TIBL top or could correspond to the top of a residual layer.
- $Zi_{NP3_{sub}}$: estimated for $NP3$ as described in Table 3, but without limit on secondary NPx maximum and NPx limit value which considers only the median profile. This configuration allows us to search for levels lower than the estimates made with a standard configuration, which could correspond to a TIBL top, or expected Zi if standard configurations assign on a residual layer top.

Our best proposed estimate is $Zi_{NP3_{std}}$, for the reasons explained before. But the four estimates embed the large complexity that is often observed in the lower troposphere.

In order to qualify this complexity and to facilitate the correct use of the four estimates, a quality flag is defined :

- flag = 1: all attributions are equal. It indicates a very good confidence in the assignment quality and a textbook case.
- flag = 2: only $Zi_{NP3_{std}}$, $Zi_{NP0_{std}}$ and $Zi_{NP3_{sub}}$ are equal. It indicates a good confidence in the assignment quality and the likely presence of a residual layer above Zi, which it would be located at $Zi_{NP0_{sup}}$. It also indicates that the Zi estimate does not match with the height of the C_n^2 maximum.

- flag = 3: only $Zi_{NP3_{std}}$, $Zi_{NP0_{std}}$ and $Zi_{NP0_{sup}}$ are equal. It indicates a medium confidence in the assignment quality and the likely presence of a TIBL located at $Zi_{NP3_{sub}}$.
- flag = 4: only $Zi_{NP3_{std}}$, $Zi_{NP0_{std}}$ are in exact agreement. It indicates a medium confidence in the assignment quality and the likely presence of both a TIBL and a residual layer, located at $Zi_{NP3_{sub}}$ and $Zi_{NP0_{sup}}$, respectively.
- flag = 5: no agreement between the four attributions of heights. This indicates poor confidence in the assignment quality, and a highly complex case.

Others flags could be produced, in order to more thoroughly document the meaning of those various estimates. They could for example qualify the temporal continuity of $Zi_{NP3_{std}}$ (occurrence of abrupt changes,...) or the consistency of $Zi_{NP3_{std}}$ with Zi_{ε}.

4 Results

4.1 Example case studies

All the assignments made by the four sets of Zi estimates are shown in the Fig. 2, Fig. 4 and Fig. 7.

4.1.1 Clear sky case

We note the very high consistency between the four different estimates in the clear sky case shown in Fig. 2. Therefore, $Zi_{NP3_{std}}$ has a good confidence index, except around 15:30 UTC, where $Zi_{NP0_{std}}$ is slightly lower than $Zi_{NP3_{std}}$. Figure 3 shows data from a radiosonde launched at 13:35 UTC the same day at CRA. In a subjective way, we estimate Zi at about 550 m, where a strong potential temperature gradient is observed, associated with a strong humidity gradient (mixing ratio and relative humidity). This height is in good agreement with all the estimates made by CALOTRITON. This is a textbook example of a typical clear sky case (see the nearly undisturbed diurnal course of the incoming shortwave radiation in Fig. 2), with flag = 1 for most of the day.

4.1.2 Cloudy complex case

For the more complex case shown in Fig. 4, the four different Zi estimates are consistent only until 11:00 UTC. After this time, $Zi_{NP0_{std}}$ and $Zi_{NP0_{sup}}$ are higher than $Zi_{NP3_{std}}$ and $Zi_{NP3_{sub}}$, suggesting that the latters may be assigned on the top of a TIBL. After 11:30 UTC, the assignments based on $NP3$ become more discontinuous due to the limit of NPx values (NPx profile mean). This discontinuity indicates an increased uncertainty in the attributions. $Zi_{NP0_{sup}}$ is then systematically located above the others, suggesting that $Zi_{NP3_{std}}$ may potentially identifiy the top of a TIBL. However, we believe that these attributions are correct, as they are located at the height where the strongest wind shear is observed.

Between 14:00 UTC and 15:00 UTC we find more continuous attributions of $Zi_{NP3_{std}}$. Data from a radiosonde taken at 14:15 UTC are shown in Fig. 3h to 3n. In a subjective way, Zi can be estimated at 1500 m, the height where the atmosphere

https://doi.org/10.5194/amt-2023-95
Preprint. Discussion started: 23 May 2023

starts to be stable (positive θ gradient), also associated with a strong discontinuity in the mixing ratio profile. This height corresponds well to $Zi_{NP3_{std}}$. We also note that $Zi_{NP0_{sup}}$ seems to correspond to the top of a residual layer around 1500 m, identified by a strong potential temperature gradient. $Zi_{NP0_{std}}$ is not successful because of the limit on the NPx values. There is also no marked local maximum of C_n^2 at the height of Zi estimated from the in-situ radiosonde, while the σ_w profile has a well marked local minimum, forming a marked local maximum on NP3.

After 15:00 UTC, Fig. 4 shows more discontinuity on $Zi_{NP3_{std}}$ attributions, demonstrating a CBL complexity with small incoming shortwave radiation, no positive sensible heat flux and rain precipitation characterized by high C_n^2 values.

This example illustrates the benefit of taking σ_w into account via NPx at $x > 0$ in the attribution of Zi. It also shows the advantage of the various Zi estimates to identify different interfaces in the case of complex vertical structure.

4.1.3 Clear sky with multiple layering

The use of the LIAISE dataset (Boone et al., 2021) allows us to test the CALOTRITON algorithm with the same UHF RWP at a different location and under different meteorological conditions. During the LIAISE campaign, the P2OA RWP was deployed from June 2021 to October 2021 in the semi arid region of Lleida, Spain, at a distance of about 15 km from large areas of irrigated crops.

Figure 7 exemplifies the complexity that can be observed in clear sky conditions in this region, and proves the capability of CALOTRITON under CBL multilayering conditions. Between 10:00 UTC and 13:00 UTC, $Zi_{NP3_{sub}}$ indicates the potential presence of a TIBL located below 1000 m. At 11:00 UTC, $Zi_{NP0_{std}}$ is at the level of $Zi_{NP3_{sub}}$ at about 600 m. Figure 8 shows measurements from a radiosonde taken at this time. In the first 1500 m, we notice the presence of two superimposed layers with constant potential temperatures and mixing ratio (Fig. 8a and 8b), separated by a thermal inversion at 600 m. Strictly speaking, according to the definition of the thermodynamic approach, Zi should be located at the top of the first layer, since the surface over-adiabaticity (28°C) theoretically does not allow a parcel of air to cross the inversion at 600 m (29°C above). By a scalar concentration approach, Zi could also be attributed to 600 m where a discontinuity in the mixing ratio is indeed observed. The latter is, however, not considered very strong and the fact that a constant mixing ratio is observed above and up to 1300 m, indicates that mixing seems to take place up to this height. The mixing may actually be horizontally homogeneous, with some turbulence structures able to overcome the inversion, and some others not. We indeed find high turbulence values ($\varepsilon > 5 \times 10^{-4}$ m^2 s^{-3}) up to 600 m. Measurements from another instrumented site, located 30 km northwest in the irrigated area, indicate a boundary layer height of 200 m at this same time. Figure 7b shows that the cooler and moister air observed over the dry site, where the RWP is located, comes from the irrigated area. Confronting these radiosonde data with the UHF RWP data, we suspect Zi at 1300 m, as $Zi_{NP3_{std}}$, with the presence of a TIBL whose top would be located at 600 m and detected by $Zi_{NP3_{sub}}$ and $Zi_{NP0_{std}}$. This example illustrates the complexity of assigning Zi with radiosonde data when several boundary layers interact, and lead to multilayering of the lower troposphere.

In Figure 7d, shortly after 13:00 UTC we notice a sudden increase in turbulence up to more than 2000 m a. g. l.. This may be due to another boundary layer advection as the wind direction (see Fig. 7b) suddenly changes from $\sim$ 200° to $\sim$ 90° between $\sim$ 1000 m and $\sim$ 2000 m. A break in the temporal continuity of $NP3$ local maxima is then observed and the imposed growth

https://doi.org/10.5194/amt-2023-95
Preprint. Discussion started: 23 May 2023

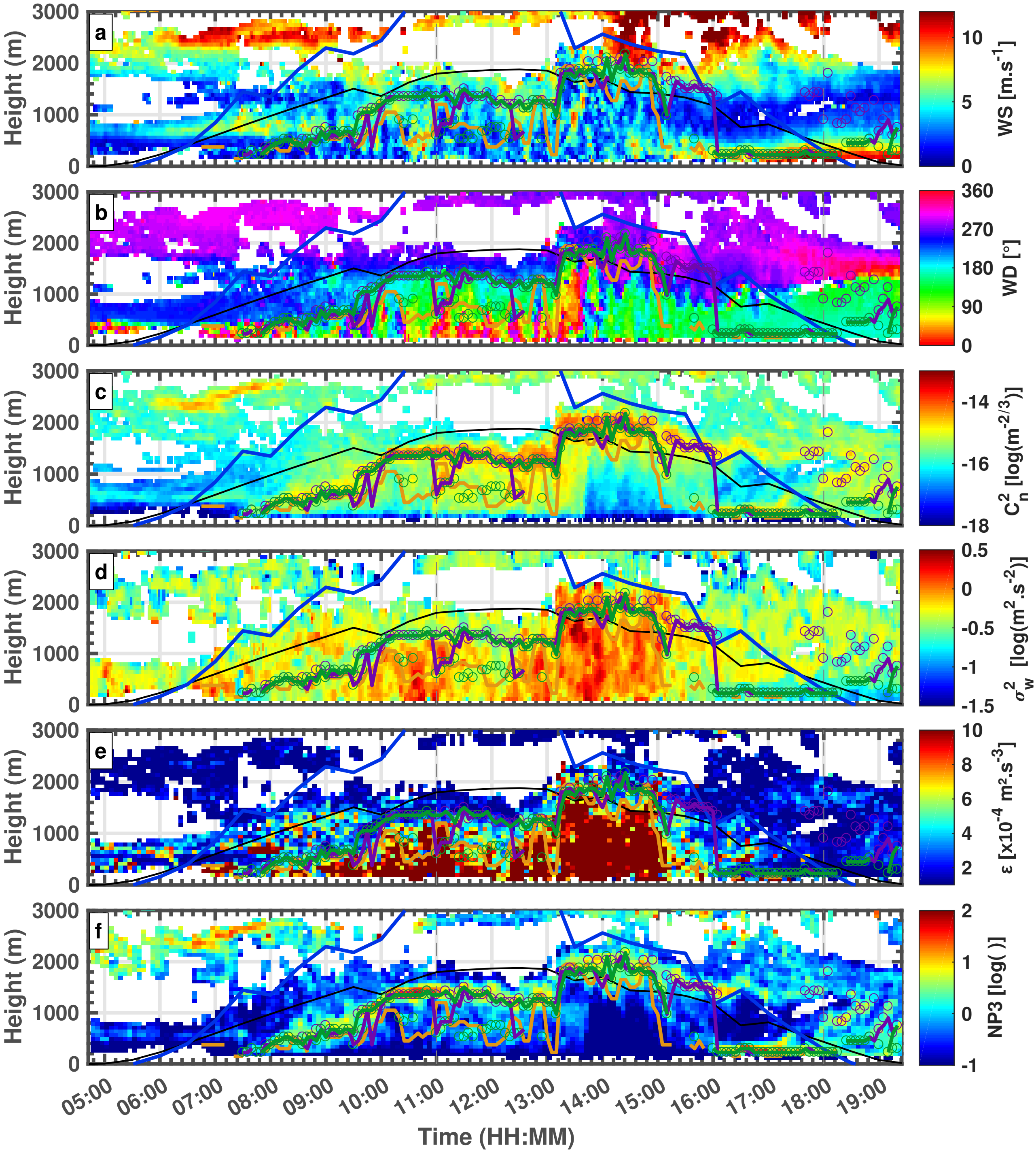

Figure 7. P2OA UHF RWP observations for 27 July 2021 at Els Plan (Spain) during the LIAISE campaign with the same description as Fig. 2, and in addition, Zi from in-situ radiosounding estimation: from parcel method (blue '+'), from potential temperature gradient method (pink '+'), from relative humidity gradient method (orange '+'), from mixing ratio gradient method (green '+'), from subjective method (black '+').

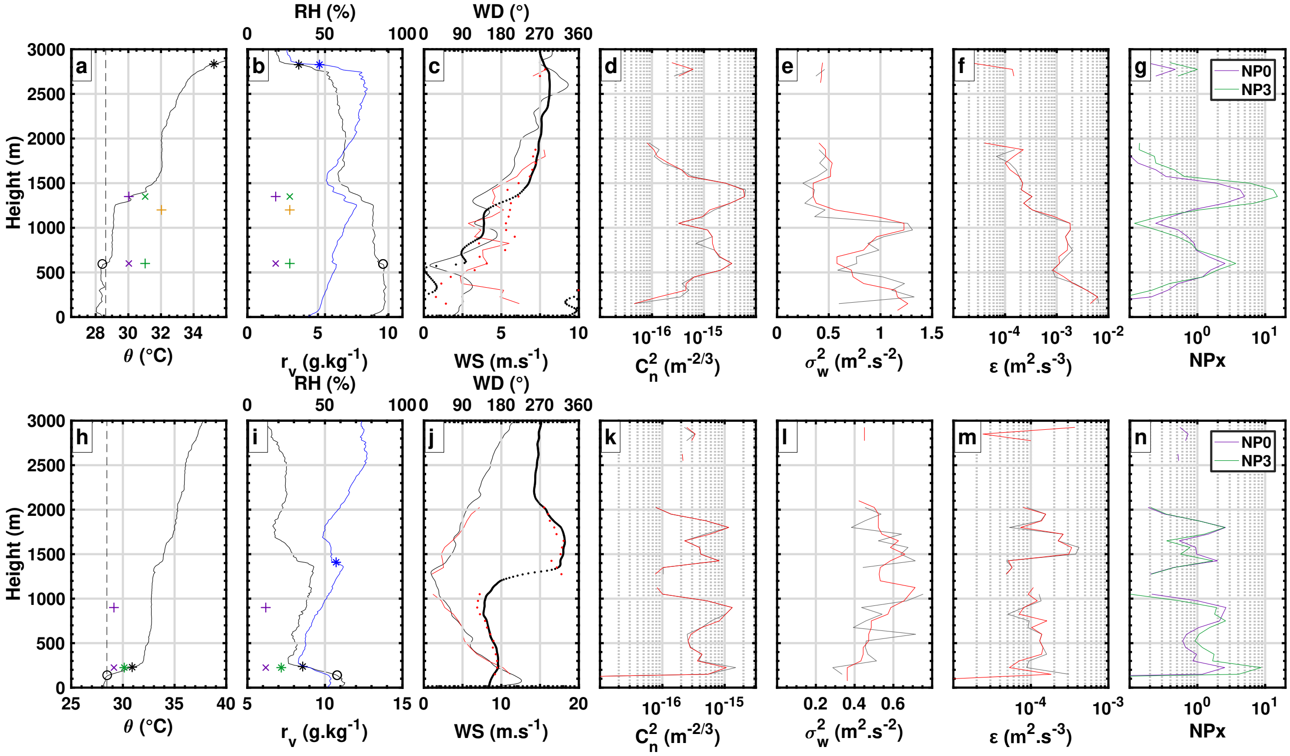

Figure 8. Same as Fig. 3, but with profiles measured by radiosounding and P2OA UHF RWP at Els Plan (Spain) during the LIAISE campaign on 27 July 2021, (a)-(g) at 11:00 UTC, and (g)-(n) at 18:00 UTC.

limit does not allow to follow this sudden evolution. The use of Zi_{ε} (1875 m at 13:15 UTC) allows attibutions of $Zi_{NP3_{std}}$ and $Zi_{NP0_{std}}$ to follow this evolution from 975 m at 13:10 UTC to 1800 m at 13:20 UTC.

From 14:00 UTC onwards, a low-level marine breeze (< 500 m) can be seen on the Fig. 7a and 7b. Between 15:00 UTC and 16:00 UTC, differences between $Zi_{NP3_{std}}$ and $Zi_{NP0_{std}}$ are observed, showing the high complexity of the atmosphere. After 16:00 UTC, all the attributions are made at 225 m on the first UHF RWP gate. Figure 8h to 8n shows the data from a radiosonde launched at 18:00 UTC where it can be seen that $Zi_{NP3_{std}}$ and $Zi_{NP0_{std}}$ are well established at the height of the maximum potential temperature and mixing ratio gradient. The observed breeze has therefore set up a new convective boundary layer.

At 19:00 UTC, the radiosonde data indicate that Zi decreases below the first reliable RWP gate, CALOTRITON attributions are then overestimated at about 500 m a. g. l.. This example has shown a highly complex situation, which can still occur in clear sky, and where the different CALOTRITON attributions can help identifying CBL top, TIBL top, and the advection of internal boundary layers. The flag defined in Sect. 3.3.3 helps to identify the days when this kind of complex layering of the low troposphere may occur.

4.2 Comparison with in-situ measurements

The previous sections have shown that $Zi_{NP3_{std}}$ gives the best estimates of Zi. To validate this result, all CALOTRITON attributions were compared to radiosonde data from the LIAISE and BLLAST campaigns with two UHF RWPs for each campaign (Table 1). During BLLAST, the CNRM UHF RWP was installed about 3 km from the P2OA-CRA UHF RWP, at Capvern. In-situ soundings were made at P2OA-CRA and Capvern with balloons (Lothon et al., 2014; Legain et al., 2013), and RPAS (Reuder et al., 2016; Båserud et al., 2020). During LIAISE, the P2OA UHF RWP was installed on the dry area (Els Plan), and the CNRM UHF RWP over the irrigated area (La Cendrosa) (see Sect. 4.1.3). Radiosoundings were launched from the two sites. A total of about 500 profiles are available for the evaluation of the CALOTRITON estimates. In-situ profiles are sometimes difficult to interpret, notably in case of complex situations like the example previously discussed (Fig. 8). Therefore, we apply different methods to estimate Zi from in-situ radiosounding or RPAS profiles. Median filters are applied to the in-situ data to match a vertical resolution of 10 m. The comparison of $Zi_{NP3_{std}}$ with the in-situ estimates, according to the method used to estimate Zi with in-situ thermodynamical data is shown in Fig. 9, and discussed in the following.

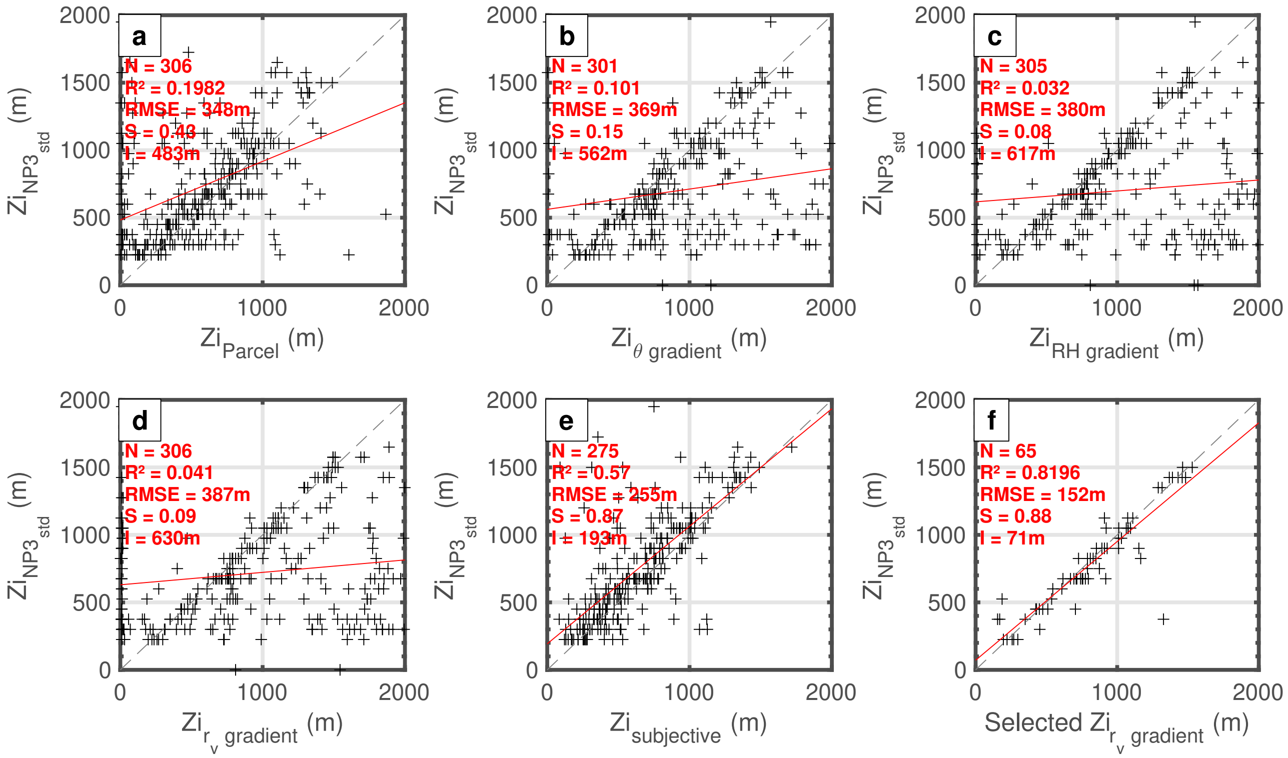

Figure 9. Attribution comparison between $Zi_{NP3_{std}}$ and (a) Zi from in-situ parcel method, (b) Zi from in-situ potential temperature gradient method, (c) Zi from in-situ relative humidity gradient method, (d) Zi from in-situ mixing ratio gradient method, (e) selected Zi from in-situ mixing ratio gradient method as described in Sect. 4.2.4. For all panels, (grey dashed line) the slope 1/1, the corresponding linear regression (red line) with its characteristics (red text): the number of data points (N), its regression coefficient (R^2), its root mean squarred error ($RMSE$), its regression slope (S) and its intercept (I).

Table 4 summarizes the results of the UHF RWP / in-situ comparison with the various CALOTRITON Zi estimates.

4.2.1 Comparison of CALOTRITON with in-situ parcel method

In the parcel method, a small amount $\delta\theta$ is added to the surface potential temperature (θ_s), and Zi_{parcel} is defined as the height where $\theta = \theta_s + \delta\theta$ above surface (Seibert et al., 2000). In this study we set $\delta\theta$ as 0.25°C.

These in-situ Zi estimates are compared to $Zi_{NP3_{std}}$ results in Fig. 9a. A great disparity of points is observed, which is mainly explained by a poor estimation of Zi_{parcel} in non-textbook cases. They are indeed either overestimated (example in Fig. 3h), or underestimated by the potential presence of TIBL (example in Fig. 8a) or by an underestimation of $\delta\theta$, also according to the intensity of the surface layer super-adiabatism.

In addition, a multitude of small Zi estimates by the parcel method (< 200 m) can be observed due to the observation of a positive potential temperature gradient in the very first meters of the profiles. Hennemuth and Lammert (2006) attribute this to evening transitions, but it may actually happen at any time (see Fig. 8h), for example by the establishment of local breezes or other advection of stable air masses.

4.2.2 Comparison of CALOTRITON with in-situ gradient methods

The gradient methods assign Zi at the height of the strongest gradient of potential temperature, water vapor mixing ratio or relative humidity, below 3000 m. Figure 9b, 9c and 9d show the comparison of those in-situ Zi estimates with $Zi_{NP3_{std}}$.

There is a large majority of cases where attributions based on gradient methods are largely above $Zi_{NP3_{std}}$. They mostly correspond to attributions to residual layers as described by Hennemuth and Lammert (2006). Also a significant number of attributions by gradient methods are very low and correspond to stable surface layer (around morning or evening transitions) as previously stated, but also to the fact that we can have large fluctuations in the surface layer, notably in water vapour mixing ratio, as we can see in Fig. 3i.

Thus, Sections 4.2.1 and 4.2.2 show that it remains difficult to qualify CALOTRITON estimates with the objective (or at least automatically determined) estimates from in-situ parcel and gradient methods.

4.2.3 Comparison of CALOTRITON with in-situ subjective method

For this reason, a subjective method of assigning Zi from in-situ thermodynamical profiles was used. This method remains as objective as possible, by assigning Zi at the height where we observe a first notable discontinuity in the mixing ratio profile associated with discontinuity in the potential temperature profile. The approach is similar to searching for the top of a conserved scalar tracer, and it should also correspond to the height where the entrainment zone starts (see Fig. 1d).

Figure 9e shows the comparison of these Zi obtained by these methods and those done by CALOTRITON using $NP3_{std}$. We start to have a good concordance between the attributions with the higter regression coefficient ($R^2 = 0.57$), but some points deviate from the trend and may be due to subjective misinterpretation as we have seen in the presence of TIBL for example.

4.2.4 Optimized comparison with selected in-situ Zi

In order to disregard errors in the in-situ estimates, we propose to restrict the $Zi_{NP3_{std}}$ / in-situ comparison to the cases where the standard deviation within the estimates from the various in-situ methods is smaller than 100 m. This way, we ensure consistency between those methods, that is, we keep more "simple" or "textbook" situations. Figure 9e shows an excellent comparison between $Zi_{NP3_{std}}$ and Zi from in-situ mixing ratio gradient method in those conditions, with R^2 = 0.82 and a root mean squarred error ($RMSE$) of 152 m that is twice the vertical resolution of the UHF RWP. However, there are still a few points that depart, which are mainly due to:

- late afternoon conditions, when the atmosphere starts to stabilize in the surface layer. In these cases, we are actually at the limit of the CBL definition;
- attributions below the UHF RWP vertical detection limitation.

If we ignore in-situ attributions below 225 m and times later than 16:00 UTC, we obtain R^2 = 0.93 and $RMSE$ = 88 m (that is close to the 75 m UHF RWP vertical resolution), which confirms the consistency of CALOTRITON estimates in those conditions.

Table 4 summarises all the comparisons made between the UHF RWP CALOTRITON estimates (based on various orders of NPx in standard configuration as described in Table 3) and in-situ estimates (based on the different methods). $Zi_{NP4_{std}}$ has a slightly larger R^2 and lower $RMSE$. However, $NP3_{std}$-based attributions are very similar to $NP4_{std}$-based attributions, and moreover lead to 4% additional attributions when compared to the subjective method in-situ estimates. This further supports the optimum choice of using $Zi_{NP3_{std}}$ to estimate Zi with CALOTRITON, and the validity of those estimates.

Finally, we have also shown that CALOTRITON is not specific to one UHF RWP and one observational site.

5 Conclusion

To conclude, we discuss each of the CALOTRITON initial objectives :

- (1) To restrict attribution in CBL case: we finally restricted the attribution as little as possible. Only the use of a humidity sensor at 2 m and a threshold value of 90% relative humidity is kept in order to avoid assigning Zi to the top of stratus returning a strong signal in NPx. The precipitation suppression function based on a threshold in C_n^2 and on the vertical velocity allows to avoid virga, which could not be detected with a rain gauge.
- (2) To manage complex cases: taking into account both the higher reflectivity at inversions and the amount of turbulence within the CBL with the use of NPx allows to improve the attributions in particular in the presence of clouds. A choice of x = 3 or 4 seems to be the most appropriate. The flag system also allows to better qualify the state of the atmosphere and gives information on the quality and difficulty of the attribution. In complex cases, characterizing the convective boundary layer by a single height may not be appropriate, in particular in the presence of TIBL where it is difficult to

https://doi.org/10.5194/amt-2023-95
Preprint. Discussion started: 23 May 2023

Table 4. Summary of linear regression characteristics between Zi from CALOTRITON with NPx (x = 0 to 5) in standard configuration as described in Table 3 and Zi from in-situ subjective method, selected Zi from in-situ mixing ratio gradient method as described in Sect. 4.2.4 and selected Zi from in-situ mixing ratio gradient method as described in Sect. 4.2.4 without taking account attributions below 225 m and only before 16:00 UTC

Compared $Zi_{NPx_{config}}$	$Zi_{NP0_{std}}$	$Zi_{NP1_{std}}$	$Zi_{NP2_{std}}$	$Zi_{NP3_{std}}$	$Zi_{NP4_{std}}$	$Zi_{NP5_{std}}$	$Zi_{NP3_{std}}(flag=1)$
	with $Zi_{subjective}$						
Number of data points	288	284	286	275	264	254	142
R^2	0.43	0.56	0.47	0.57	0.59	0.56	0.62
$RMSE$	285 m	246 m	309 m	255 m	253 m	270 m	255 m
Slope	0.74	0.85	0.86	0.87	0.89	0.89	0.9
Intercept	219 m	162 m	204 m	193 m	193 m	200 m	150 m
	with selected $Zi_{r_v gradient}$						
Number of data points	68	68	67	65	64	61	37
R^2	0.67	0.74	0.65	0.82	0.88	0.88	0.94
$RMSE$	204 m	178 m	206 m	152 m	119 m	128 m	94 m
Slope	0.81	0.82	0.76	0.88	0.9	0.93	0.96
Intercept	81 m	95 m	162 m	71 m	81 m	56 m	4 m
	with selected $Zi_{r_v gradient}$ without Zi <225 m and only before 16:00 UTC						
Number of data points	52	52	51	49	49	49	26
R^2	0.72	0.81	0.82	0.93	0.94	0.90	0.96
$RMSE$	184 m	144 m	139 m	88 m	82 m	109 m	80 m
Slope	0.99	0.99	0.99	1.02	1.02	1.04	1.02
Intercept	-86 m	-46 m	-46 m	-39 m	-30 m	-54 m	-47 m

determine Zi, even based on in-situ thermodynmical data. It becomes very difficult to statistically qualify CALOTRITON attributions in such cases. An intercomparison of the results of the StratFinder algorithm (Kotthaus et al., 2020) applied on a newly installed Vaisala CL61 ceilometer at P2OA-CRA with the CALOTRITON estimates is planned in order to better characterize Zi attributions by CALOTRITON in complex cases, but also to better understand the differences between the scalar concentration approach, a thermodynamical approach or a turbulence approach in relation with the CBL processes.

- (3) To respect temporal continuity of Zi development: although it is not emphasized in this paper, the fact of restricting the first attribution of Zi to the first reliable UHF RWP gate is a significant progress. Indeed, the technique presented by Angevine et al. (1994) assigns Zi at the height of the maximum reflectivity without taking into account the potential presence of a residual layer in the morning, like is the case in Fig. 7c between 07:00 UTC and 08:00 UTC at about 2500 m. Nevertheless, attribution errors are still observed, essentially in the morning when the residual layers are close to the actual Zi and the relative threshold of the secondary maximum of NPx (90% before 10:00 UTC) is not sufficient. In contrary, in the afternoon, Zi usually reaches a plateau. We could have constrained the attributions around the last allocated Zi and thus avoided taking into account a relative difference between the local maximums of NPx, which adds complexity to the algorithm. However, this choice would not have allowed us to detect the apparition of a new

https://doi.org/10.5194/amt-2023-95
Preprint. Discussion started: 23 May 2023

convective boundary layer as we have seen for the LIASIE campaign. Finally the empirical choice of growth limit values associated with the relative thresholds of secondary maximum of NPx gives convincing results.

- (4) To take into account abrupt CBL growth: using Zi_ε to allow larger growth limit helps to better manage complex cases but it was noticed that it can also generate errors, in particular in the morning, by attributing Zi at the height of residual layers. Using an additional median filter on Zi_ε makes it possible to limit these errors by better considering a certain temporal continuity of Zi_ε. The choice of a threshold in ε for Zi_ε estimate is, however, not the most appropriate. An improvement could be brought on that aspect. An intercomparison could also be made between lidar and UHF RWP instruments.
- (5) To use limited instrumental synergy: only two additional instruments are used in addition to the UHF RWP: a humidity sensor at 2 m and sonic anemometers for the evaluation of the sensible heat flux. The latter could, however, be ignored since the method of searching for the t_{init} based on the value of C_n^2 at the first gate of the UHF RWP still gives satisfying results. On the other hand, the use of the humidity sensor allows to strongly restrict the attributions, especially in the presence of low stratus and fog, and remains an easy and low cost solution. The set of attributions must also be further restricted, especially when Zi gets below the RWP lower vertical limit, when the boundary layer initiates its night transition. Moreover, sensible heat flux data can be used to only keep the estimates of Zi in the presence of positive flux. However, this choice has not been made at P2OA-CRA, whose location at the foot of the Pyrenees is subject to Foehn winds, potentially resulting in daytime negative sensible heat flux measurements (but positive latent heat flux) in the surface layer.

We have not addressed so far the difficulty of attribution of Zi during the winter period, which will be primarily due to small Zi, often below the lower detection limit of the UHF RWP, but also to reduced cover range of the RWP in a much drier atmosphere. The choice of dividing the NPx by the profile mean initially aimed at working with dimentionless variable but also at applying this algorithm to uncalibrated UHF RWP reflectivities. It remains interesting to regularly calibrate it, in order to optimize the threshold of C_n^2 for the precipitation periods removal.

Finally, the main objective of obtaining reliable estimates of Zi with a UHF RWP, for the analysis of long term series, is met.

Code availability.

CALOTRITON code is available from the authors upon request.

Data availability.

Table 1 summarises the data availability. Only the CT25k ceilometer data are available from the authors upon request.

Author contributions.

AP is the main author of CALOTRITON algorithm: conception, coding, tests, evaluation, data analysis. He is also the main writer of the article. ML supervised the work and analysis, and helped in the writing. She is the principal investigator of the P2OA UHF RWP. JA and PYM are the coordinators of the funding contract, and collaborated to the work. BC is the author of the initial code for the UHF RWP data process, and of the previous algorithm for Zi estimates. He helped to the algorithm conception. SD is responsible for the P2OA-CRA instrumentation and data. She and AV helped in instrumentation maintenance, data process, and data availability. YB operates the P2OA UHF RWP, and helpd in the operation of the CNRM UHF RWP during LIAISE. FL is the principal investigator of the 60 m tower, and contributed to the writing. GC was the lead of the instrumental deployment during LIAISE, especially of the CNRM instruments installed at La Cendrosa. JB was responsible for the deployment of radiosoundings at Els Plan during LIAISE, and contributed to the writing. JR was the PI of SUMO RPAS during BLLAST, and contributed to the writing.

Competing interests.

The contact author has declared that neither of the authors has any competing interests.

Acknowledgements. We gratefully acknowledge the French Atomic Energy Commission (CEA) assisted by the Université Paul Sabatier, Toulouse, for funding this study and their support.

P2OA-CRA observation data were collected at the Pyrenean Platform for Observation of the Atmosphere P2OA (http://p2oa.aero.obs-mip.fr). P2OA facilities and staff are funded and supported by the University Paul Sabatier Toulouse 3, France, and CNRS (Centre National de la Recherche Scientifique). P2OA is a component of the ACTRIS-Fr Research Infrastructure and benefits from AERIS data centre (https://www.aeris-data.fr/) for hosting service data. The 60 m tower is partly supported by the POCTEFA/FLUXPYR European program.

The BLLAST field experiment was made possible thanks to the contribution of several institutions and supports : INSU-CNRS (Institut National des Sciences de l'Univers, Centre national de la Recherche Scientifique, LEFE-IDAO program), Météo-France, Observatoire Midi-Pyrénées (University of Toulouse), EUFAR (EUropean Facility for Airborne Research) and COST ES0802 (European Cooperation in the field of Scientific and Technical). The field experiment would not have occurred without the contribution of all participating European and American research groups, which all have contributed in a significant amount (see https://bllast.aeris-data.fr/bllast-supports/). The BLLAST field experiment was hosted by the instrumented site of Centre de Recherches Atmosphériques, Lannemezan, France (Observatoire Midi-Pyrénées, Laboratoire d'Aérologie). BLLAST data are managed by SEDOO, from Observatoire Midi-Pyrénées. The French ANR (Agence Nationale de la Recherche) supported BLLAST analysis in the 2013-2015 BLLAST-A project. The french contribution to the LIAISE project has been supported by ANR HILIAISE and Meteo-France. We acknowledge Gilles André, Géraldine Pagan, Vinciane Unger, Alain Dabas, Alexandre Paci, and GMEI/LISA team of CNRM UMR. We also acknowledge Jeremy Price and all the Met Office team involved in LIAISE.

References

Angevine, W. M., White, A. B., and Avery, S. K.: Boundary-layer depth and entrainment zone characterization with a boundary-layer profiler, Boundary-Layer Meteorology, 68, 375–385, https://doi.org/10.1007/BF00706797, 1994.

Blay-Carreras, E., Pino, D., Arellano, J. V.-G. D., Boer, A. V. D., Coster, O. D., Darbieu, C., Hartogensis, O., Lohou, F., Lothon, M., and Pietersen, H.: Role of the residual layer and large-scale subsidence on the development and evolution of the convective boundary layer, Atmospheric Chemistry and Physics, 14, 4515–4530, https://doi.org/10.5194/acp-14-4515-2014, 2014.

Boone, A., Bellvert, J., Best, M., Brooke, J., Canut-Rocafort, G., Cuxart, J., Hartogensis, O., Moigne, P. L., Miró, R., and Polcher, J.: Updates on the International Land Surface Interactions with the Atmosphere over the Iberian Semi-Arid Environment (LIAISE) Field Campaign, https://hal.science/hal-03842003, 2021.

Båserud, L., Reuder, J., Jonassen, M. O., Bonin, T. A., Chilson, P. B., Jiménez, M. A., and Durand, P.: Potential and Limitations in Estimating Sensible-Heat-Flux Profiles from Consecutive Temperature Profiles Using Remotely-Piloted Aircraft Systems, Boundary-Layer Meteorology, 174, 145–177, https://doi.org/10.1007/s10546-019-00478-9, 2020.

Caicedo, V., Rappenglück, B., Lefer, B., Morris, G., Toledo, D., and Delgado, R.: Comparison of aerosol lidar retrieval methods for boundary layer height detection using ceilometer aerosol backscatter data, Atmospheric Measurement Techniques, 10, 1609–1622, https://doi.org/10.5194/amt-10-1609-2017, 2017.

Canut, G., Garrouste, O., and Etienne, J.-C.: LIAISE LA-CENDROSA CNRM MTO-1MIN L2. [DataSet]., https://doi.org/https://doi.org/10.25326/33, 2022.

Cohn, S. A. and Angevine, W. M.: Boundary Layer Height and Entrainment Zone Thickness Measured by Lidars and Wind-Profiling Radars, Journal of Applied Meteorology, 39, 1233–1247, https://doi.org/10.1175/1520-0450(2000)039<1233:BLHAEZ>2.0.CO;2, 2000.

Couvreux, F., Bazile, E., Canut, G., Seity, Y., Lothon, M., Lohou, F., Guichard, F., and Nilsson, E.: Boundary-layer turbulent processes and mesoscale variability represented by numerical weather prediction models during the BLLAST campaign, Atmospheric Chemistry and Physics, 16, 8983–9002, https://doi.org/10.5194/acp-16-8983-2016, 2016.

Davis, K. J., Gamage, N., Hagelberg, C., Kiemle, C., Lenschow, D., and Sullivan, P.: An objective method for deriving atmospheric structure from airborne lidar observations, Journal of Atmospheric and Oceanic Technology, 17, 1455–1468, 2000.

Deardorff, J. W.: Theoretical expression for the countergradient vertical heat flux, Journal of Geophysical Research, 77, 5900–5904, https://doi.org/10.1029/jc077i030p05900, 1972.

Doviak, R. and Zrnic, D.: Doppler Radar and Weather Observations, Elsevier, https://doi.org/10.1016/C2009-0-22358-0, 1993.

Duncan, J. B., Bianco, L., Adler, B., Bell, T., Djalalova, I. V., Riihimaki, L., Sedlar, J., Smith, E. N., Turner, D. D., Wagner, T. J., and Wilczak, J. M.: Evaluating convective planetary boundary layer height estimations resolved by both active and passive remote sensing instruments during the CHEESEHEAD19 field campaign, Atmospheric Measurement Techniques, 15, 2479–2502, https://doi.org/10.5194/amt-15-2479-2022, 2022.

Durand, P., Druilhet, A., and Briere, S.: A Sea-Land Transition Observed during the COAST Experiment, Journal of the Atmospheric Sciences, 46, 96–116, https://doi.org/10.1175/1520-0469(1989)046<0096:ASLTOD>2.0.CO;2, 1989.

Frehlich, R., Meillier, Y., Jensen, M. L., Balsley, B., and Sharman, R.: Measurements of Boundary Layer Profiles in an Urban Environment, Journal of Applied Meteorology and Climatology, 45, 821–837, https://doi.org/10.1175/JAM2368.1, 2006.

Garrouste, O.: UHF CNRM Site 2. [Dataset], https://doi.org/https://doi.org/10.6096/bllast.uhf.site2, 2011.

Garrouste, O., Canut, G., and Roy, A.: LIAISE LA-CENDROSA CNRM RS L2. [Dataset]., https://doi.org/https://doi.org/10.25326/322, 2022.

Haeffelin, M., Angelini, F., Morille, Y., Martucci, G., Frey, S., Gobbi, G. P., Lolli, S., O'Dowd, C. D., Sauvage, L., Xueref-Rémy, I., Wastine, B., and Feist, D. G.: Evaluation of Mixing-Height Retrievals from Automatic Profiling Lidars and Ceilometers in View of Future Integrated Networks in Europe, Boundary-Layer Meteorology, 143, 49–75, https://doi.org/10.1007/s10546-011-9643-z, 2012.

Hennemuth, B. and Lammert, A.: Determination of the atmospheric boundary layer height from radiosonde and lidar backscatter, Boundary-Layer Meteorology, 120, 181–200, https://doi.org/10.1007/s10546-005-9035-3, 2006.

Heo, B.-H., Jacoby-Koaly, S., Kim, K.-E., Campistron, B., Benech, B., and Jung, E.-S.: Use of the Doppler Spectral Width to Improve the Estimation of the Convective Boundary Layer Height from UHF Wind Profiler Observations, 2000.

Holzworth, G. C.: Estimates of mean maximum mixing depths in the contiguous united states, Monthly Weather Review, 92, 235–242, https://doi.org/10.1175/1520-0493(1964)092<0235:EOMMMD>2.3.CO;2, 1964.

Jacoby-Koaly, S.: Application d'un radar profileur de vent UHF à l'étude de la couche limite atmosphérique, Ph.D. thesis, http://www.theses.fr/2000TOU30144, thèse de doctorat dirigée par Campistron, Bernard Physique de l'atmosphère Toulouse 3 2000, 2000.

Jacoby-Koaly, S., Campistron, B., Bernard, S., Bénech, B., Ardhuin-Girard, F., Dessens, J., Dupont, E., and Carissimo, B.: Turbulent Dissipation Rate In The Boundary Layer Via UHF Wind Profiler Doppler Spectral Width Measurements, Boundary-Layer Meteorology, 103, 361–389, https://doi.org/10.1023/A:1014985111855, 2002.

Kossmann, M., Gtlin, R. V., Corsmeier, U., Vogel, B., Fiedler, F., Binder, H.-J., Kalthoff, N., and Beyrich, F.: Aspects of the convective boundary layer structure over complex terrain, Atmospheric Environment, 32, 1323–1348, 1998.

Kotthaus, S., Haeffelin, M., Drouin, M. A., Dupont, J. C., Grimmond, S., Haefele, A., Hervo, M., Poltera, Y., and Wiegner, M.: Tailored algorithms for the detection of the atmospheric boundary layer height from common automatic lidars and ceilometers (Alc), Remote Sensing, 12, 1–23, https://doi.org/10.3390/rs12193259, 2020.

Legain, D.: Frequent radiosoundings Site 2. [Dataset]., https://doi.org/https://doi.org/10.6096/bllast.frequentsoundingssite2, 2011.

Legain, D., Bousquet, O., Douffet, T., Tzanos, D., Moulin, E., and Barrie, J.: High-frequency boundary layer profiling with reusable radiosondes, Atmospheric Measurement Techniques, 6, 2195–2205, https://doi.org/10.5194/amt-6-2195-2013, 2013.

Lohou, F.: Meteorological parameters and flux. [Dataset]., https://doi.org/https://doi.org/10.6096/bllast.60mtower.meteo, 2017.

Lohou, F., Derrien, S., and Vial, A.: [Dataset], https://doi.org/to be specified, to be specifieda.

Lohou, F., Derrien, S., and Vial, A.: to be specified, [Dataset], https://doi.org/to be specified, to be specifiedb.

Lothon, M.: MODEM Radiosoundings Site 1. [Dataset], https://doi.org/https://doi.org/10.6096/bllast.modem, 2018.

Lothon, M. and Vial, A.: LIAISE ELS-PLANS LAERO UHFWindProfiler-LowMode L2. [Dataset]., https://doi.org/https://doi.org/10.25326/363, 2022.

Lothon, M., Lenschow, D. H., and Mayor, S. D.: Coherence and scale of vertical velocity in the convective boundary layer from a Doppler lidar, Boundary-Layer Meteorology, 121, 521–536, https://doi.org/10.1007/s10546-006-9077-1, 2006.

Lothon, M., Lohou, F., Pino, D., Couvreux, F., Pardyjak, E. R., Reuder, J., Arellano, J. V.-G. D., Durand, P., Hartogensis, O., Legain, D., Augustin, P., Gioli, B., Lenschow, D. H., Faloona, I., Yagüe, C., Alexander, D. C., Angevine, W. M., Bargain, E., Barrié, J., Bazile, E., Bezombes, Y., Blay-Carreras, E., Boer, A. V. D., Boichard, J. L., Bourdon, A., Butet, A., Campistron, B., Coster, O. D., Cuxart, J., Dabas, A., Darbieu, C., Deboudt, K., Delbarre, H., Derrien, S., Flament, P., Fourmentin, M., Garai, A., Gibert, F., Graf, A., Groebner, J., Guichard, F., Jiménez, M. A., Jonassen, M., Kroonenberg, A. V. D., Magliulo, V., Martin, S., Martinez, D., Mastrorillo, L., Moene, A. F., Molinos, F., Moulin, E., Pietersen, H. P., Piguet, B., Pique, E., Román-Cascón, C., Rufin-Soler, C., Saïd, F., Sastre-Marugán, M., Seity, Y., Steeneveld,

G. J., Toscano, P., Traullé, O., Tzanos, D., Wacker, S., Wildmann, N., and Zaldei, A.: The BLLAST field experiment: Boundary-Layer late afternoon and sunset turbulence, Atmospheric Chemistry and Physics, 14, 10 931–10 960, https://doi.org/10.5194/acp-14-10931-2014, 2014.

Lothon, M., Gheusi, F., Lohou, F., Pont, V., Derrien, S., Bezombes, Y., Leclerc, E., Vial, A., Athier, G., Jambert, C., Gardrat, E., Andriatiana, A., Meyerfeld, Y., Campistron, B., Saïd, F., Philibert, A., Stark, F., Estrampes, J.-B., Pique, E., Guesdon, F., Bret, G., Lacassagne, F., Guesdon, L., Gueffier, J., Jeroen, S., and Zaïda, G. K.: The long-term dataset of the Pyrenean Platform for Observation of the Atmosphere, To be sumitted to Earth System Science Data, 2023.

Lothon, M., Bezombes, Y., and Vial, A.: to be specified [Dataset], https://doi.org/to be specified, to be specified.

Min, J. S., Park, M. S., Chae, J. H., and Kang, M.: Integrated System for Atmospheric Boundary Layer Height Estimation (ISABLE) using a ceilometer and microwave radiometer, Atmospheric Measurement Techniques, 13, 6965–6987, https://doi.org/10.5194/amt-13-6965-2020, 2020.

Price, J.: LIAISE ELS-PLANS UKMO MTO-30MIN L2. [Dataset]., https://doi.org/https://doi.org/10.25326/430, 2023a.

Price, J.: LIAISE ELS-PLANS UKMO radiosondes L1. [Dataset]., https://doi.org/https://doi.org/10.25326/429, 2023b.

Reuder, J. and Jonassen, M.: SUMO. [Dataset]., https://doi.org/https://doi.org/10.25326/469, 2017.

Reuder, J., Båserud, L., Jonassen, M. O., Kral, S. T., and Müller, M.: Exploring the potential of the RPA system SUMO for multipurpose boundary-layer missions during the BLLAST campaign, Atmospheric Measurement Techniques, 9, 2675–2688, https://doi.org/10.5194/amt-9-2675-2016, 2016.

Saïd, F.: LA Site 1. [Dataset], https://doi.org/https://doi.org/10.6096/bllast.uhf.site1, 2012.

Seibert, P., Beyrich, F., Gryning, S.-E., Joffre, S., Rasmussen, A., and Tercier, P.: Review and intercomparison of operational methods for the determination of the mixing height, Atmospheric environment, 34, 1001–1027, 2000.

Stull, R. B.: An Introduction to Boundary Layer Meteorology, Springer Netherlands, https://doi.org/10.1007/978-94-009-3027-8, 1988.

Vial, A.: to be specified, https://doi.org/to be specified, 2023.